

Modeling branched and intersecting faults in reservoir-geomechanics models with the extended finite element method

Chuanqi Liu^a, Jean H. Prévost^a, N. Sukumar^b

^a*Department of Civil and Environmental Engineering, Princeton University, Princeton, NJ 08544, USA*

^b*Department of Civil and Environmental Engineering, University of California, Davis, CA 95616, USA*

Abstract

Faults are geological entities with thickness several orders of magnitude smaller than the grid blocks typically used to discretize geological formations. On using the extended finite element method (X-FEM), a structured mesh suffices and the faults can arbitrarily cut the elements in the mesh. Modeling branched and intersecting faults is a challenge, in particular when the faults work as internal fluid flow conduits that allow fluid flow in the faults as well as to enter/leave the faults. By appropriately selecting the enrichment function and the nodes to be enriched, we are able to capture the special characteristics of the solution in the vicinity of the fault. We compare different enrichment schemes for strong discontinuities and develop new continuous enrichment functions with discontinuous derivatives to model branched and intersecting weak discontinuities. Symmetric fluid flows within the regions

Email address: chuanqil@hotmail.com, chuanqil@princeton.edu (Chuanqi Liu)

embedded by branched, coplanar intersecting, and non-coplanar intersecting faults are considered to verify the effectiveness of the proposed enrichment scheme. For a complex fault consisting of branched and intersecting faults, the accuracy and efficiency of the X-FEM is compared to the FEM. We also demonstrate different slipping scenarios for branched and intersecting faults with the same friction coefficient. In additions, fault slipping triggered by an injection pressure and three-dimensional fluid flows are modeled to show the versatility of the proposed enrichment scheme for branched and intersecting weak discontinuities.

Keywords: branched and intersecting faults, X-FEM,
reservoir-geomechanics

1. Introduction

Faults are geological entities with thicknesses several orders of magnitude smaller than the grid blocks typically used to discretize reservoir and/or over-under-burden geological formations (Prévost et al., 2017). For geomechanics, the fault as an internal displacement discontinuity that allows slipping to occur. For reservoir, the fault is either an internal fluid flow conduit that allows fluid flow in the fault as well as to enter/leave the fault or is a barrier to flow (Martin et al., 2005). Prévost and Sukumar (2016) proposed a three-dimensional reservoir-geomechanical model with the extended finite element method (X-FEM) to assess the potential for fault reactivation. However, the modeling of branched and intersecting faults, in particular when the faults

work as internal fluid flow conduits, remains a challenge.

The X-FEM and the generalized finite element method (GFEM) are versatile tools for the analysis of problems characterized by discontinuities, singularities, and localized deformations. Both methods are synonymous (Belytschko et al., 2009), and rely on the partition-of-unity enrichment framework of Melenk and Babuška (1996). The advantage of these methods is that the finite element mesh is constructed totally independent of the presence of discontinuities. This allows for adopting a structured mesh and inserting many (tens or even hundreds) of discontinuities since the discontinuities are never meshed. On using the X-FEM, we incorporate discontinuous enrichment functions for the standard finite element space to account for discontinuities. By appropriately selecting the enrichment function and the nodes to be enriched, the enriched approximation is capable of directly capturing the special characteristics of the solution in the local parts of the domain (Belytschko et al., 2009). For instance, the approximation of pressure should be enriched by a discontinuous function for the case of the fault working as a barrier to flow, and enriched by a continuous function with discontinuous derivatives when the fault works as a flow conduit. Hereafter, we refer to strong discontinuities when using discontinuous functions and weak discontinuities when continuous functions with discontinuous derivatives are used.

For strong discontinuities, Daux et al. (2000) proposed to add junction enrichments to the classical X-FEM enrichment for branched and intersecting discontinuities. The introduction of the discontinuities has to respect

a certain hierarchy. For modeling discontinuous grain boundaries, Simone et al. (2006) partitioned the element fully cut by a branched or intersecting crack into several regions. Each region is connected with an enrichment function whose value is unity when the spatial point is within the region and 0 elsewhere. Since the sum of all enrichment functions is unity for any point, which means one of enrichment functions can be linearly expressed by the others, the enriched DOF is one less than the number of regions. This algorithm is more general and easier to implement than the one by Daux et al. (2000) since each discontinuity is independent of the others and no junction enrichment is needed. An alternative approach to handle intersecting and branched cracks in the X-FEM is via the use of harmonic enrichment functions (Mousavi et al., 2011a,b). More alternative enrichment schemes can be found in the retrospective article by Sukumar et al. (2015). For weak discontinuities, the distance function is often used as the enrichment (Belytschko et al., 2001). Hansbo and Hansbo (2002, 2004) adopted Nitsche’s method to impose interface conditions to model weak discontinuities. However, to our knowledge, there are no prior studies that have considered branched and intersecting weak discontinuities.

In this work, we focus on the assessment of fault reactivation arising from slipping. Because the mechanism of fracturing is complex due to the existence of plastic zone, we do not consider the singular functions at the tips of faults. Hence, all enriched element are fully cut by the faults. The rest of the paper is organized as follows. We first compare the enrichment

schemes using by Daux et al. (2000) and Simone et al. (2006) for branched and intersecting strong discontinuities and present new enrichment schemes for weak discontinuities. Section 3 shows the procedure for implementing the enrichment schemes into reservoir-geomechanical models. Section 4 presents the results including symmetric fluid flows, fluid flow within complex faults, slipping of branched and intersecting faults, slipping triggered by an injection pressure and three-dimensional fluid flows. We provide some final remarks in Section 5.

2. Extended Finite Element Approximation

Let the number of nodes of a given finite element be nen , and the index set $\mathbb{I} := \{1, 2, \dots, nen\}$. The extended finite element approximation for a scalar field $u(\mathbf{x})$ in the element takes the form

$$u_e^h(\mathbf{x}) = \sum_{I \in \mathbb{I}} N_I(\mathbf{x}) u_I + \sum_{J \in \mathbb{J} \subseteq \mathbb{I}} N_J(\mathbf{x}) \psi(\mathbf{x}) a_J, \quad (1)$$

where $N_I(\mathbf{x})$ is the standard FE shape function for node I , u_I is the standard nodal DOF, \mathbb{J} is the index set of nodes whose basis function support is cut by the interior of the fault, for the element fully cut by the fault $\mathbb{J} = \mathbb{I}$, $\psi(\mathbf{x})$ is an enriched function, and a_J is the enriched DOF. The characteristics of faults can be reflected by choosing appropriate $\psi(\mathbf{x})$.

2.1. Enrichment functions for the case of strong discontinuities

In the X-FEM, the discontinuity of the approximation is introduced by the generalized Heaviside function, which is defined as

$$H(\mathbf{x}) = \begin{cases} 1 & \text{if } d(\mathbf{x}) > 0 \\ -1 & \text{if } d(\mathbf{x}) < 0 \end{cases}, \quad (2)$$

where $d(\mathbf{x})$ is the signed distance to a fault Γ^c . Following Simone et al. (2006), the union of all the nodal supports completely cut by the discontinuity (denoted as Ω_{fault}) is divided into two disjoint regions Ω_1 and Ω_2 , i.e. $\Omega_{\text{fault}} = \Omega_1 \cup \Omega_2$ and $\Omega_1 \cap \Omega_2 = \emptyset$. Two discontinuous functions $H_\alpha(\mathbf{x})$ are then defined corresponding to Ω_α ($\alpha = 1, 2$), as

$$H_\alpha(\mathbf{x}) = \begin{cases} 1 & \text{if } \mathbf{x} \in \Omega_\alpha \\ 0 & \text{otherwise} \end{cases}. \quad (3)$$

The nodes whose support intersects the discontinuity are enriched with both $H_1(\mathbf{x})$ and $H_2(\mathbf{x})$. However, $H_1(\mathbf{x})$ and $H_2(\mathbf{x})$ are linearly dependent as

$$\sum_{\alpha} H_\alpha(\mathbf{x}) = 1 \quad \forall \mathbf{x} \in \Omega_{\text{fault}}, \quad (4)$$

and hence the nodes only need to be enriched by either $H_1(\mathbf{x})$ or $H_2(\mathbf{x})$. Fig. 1 shows the comparison of one-dimensional enrichment functions for different methods. The discontinuity is located at $x = 0$.

As illustrated in Fig. 2, single, branched and intersecting faults can be represented. Also, one element may be cut by two separate faults, such as

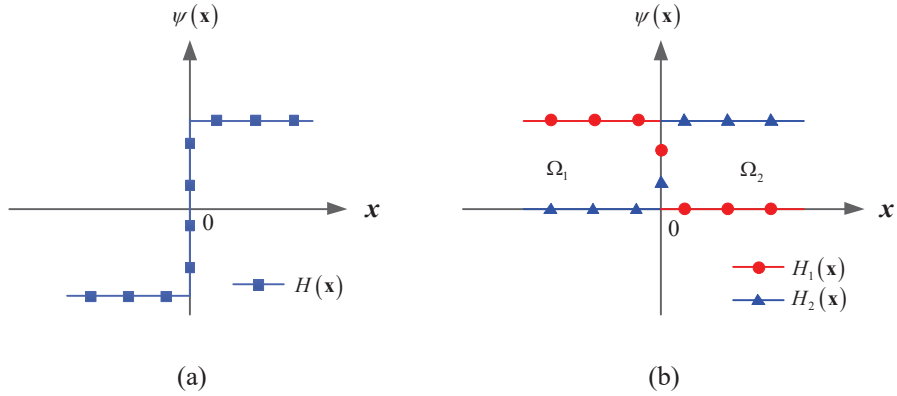


Figure 1: Enrichment functions for the case of strong discontinuities with: (a) Generalized Heaviside enrichment, and (b) step function enrichment. The discontinuity is located at $x = 0$.

elements e_1 and e_2 in Fig. 2. Hence, different enrichment schemes are needed for different cases. In Daux et al. (2000), the fault having multiple branches is treated as an intersection of a main fault and several secondary faults, and additional junction functions are needed. When the configuration of the faults is complex, the procedure is cumbersome since we have to preprocess the hierarchy of these faults. However, in the scheme due to Simone et al. (2006), there is no need for such preprocessing and the branches are independent. We only need to divide the union of nodal supports completely cut by the fault into several regions according to the configuration of the fault and assign a simple step function to each region. If we have more than one enrichment function, one of them can be eliminated since it is a linear combination of the others and the constant function. Referring to Fig. 2, the approximation for a vector field $\mathbf{u}(\mathbf{x})$ can be written as (Simone et al.,

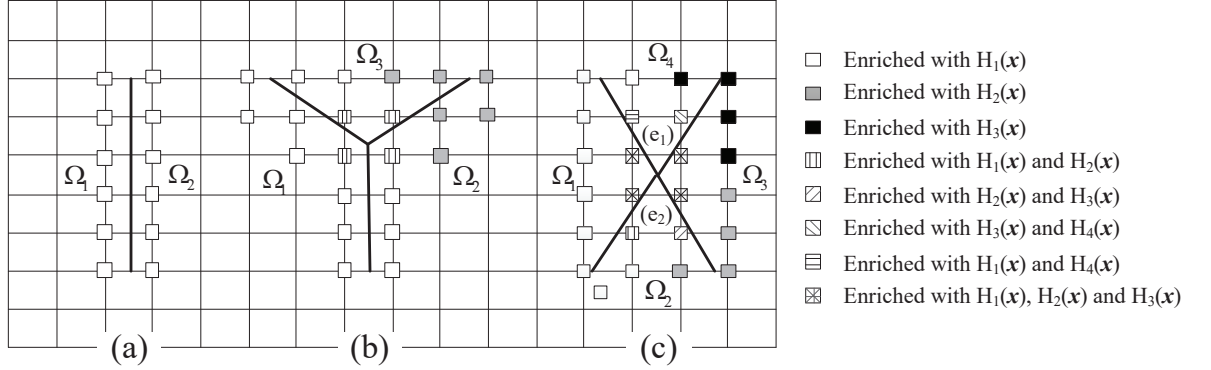


Figure 2: Enrichment functions for modeling different types of faults (a) single fault, (b) branched fault, and (c) intersecting fault.

2006),

$$\mathbf{u}_e^h(\mathbf{x}) = \sum_I N_I(\mathbf{x}) \left[\mathbf{u}_I + \sum_{\alpha=1}^n H_\alpha(\mathbf{x}) \mathbf{a}_{\alpha I} \right] \quad (5)$$

where $H_\alpha(\mathbf{x})$ is the step function of region Ω_α defined (3), and $\mathbf{a}_{\alpha I}$ is the enriched nodal DOF. Due to the linear dependence, the number of nodal enriched DOFs n is one less than the number of regions, for example, $n = 1$ for the elements cut by one fault, $n = 2$ for the elements cut by two separate faults or branched faults, and $n = 3$ for the elements cut by intersecting faults. Fig. 2 shows one optional enrichment strategy without loss of generality. For example, the node enriched by $H_1(\mathbf{x})$ and $H_2(\mathbf{x})$ can also be enriched by $H_1(\mathbf{x})$ and $H_3(\mathbf{x})$ (or $H_2(\mathbf{x})$ and $H_3(\mathbf{x})$).

In general, nodes are enriched whose support intersects a discontinuity. For nodes whose support is not intersected by a discontinuity, the nodal response for the enrichment is empty since the Heaviside function (or step function) is a constant over their supports and can be neglected. Inspired by

the enrichment strategy of Simone et al. (2006), we establish new enrichment schemes for the branched and intersecting weak faults, as described hereafter.

2.2. Enrichment functions for weak discontinuities

For the case of the fault working as a flow conduit, the pressure is continuous, whereas the flow velocity (i.e., the gradient of pressure) exhibits a jump across the fault. Then, the requirement for the enrichment function $\psi(\boldsymbol{x})$ becomes that $\psi(\boldsymbol{x})$ is continuous but the spatial gradient of $\psi(\boldsymbol{x})$ is discontinuous across the fault. For the simplest case as of a single fault, the distance function $\phi(\boldsymbol{x})$ is often enriched for the approximation, which is defined as,

$$\phi(\boldsymbol{x}) = \min \|\boldsymbol{x} - \bar{\boldsymbol{x}}\|_{\bar{\boldsymbol{x}} \in \Gamma^c}, \quad (6)$$

where Γ^c denoting the position of the fault and $\|\cdot\|$ is the norm of a vector. Fig. 3(a) depicts the one-dimensional enrichment function assuming the discontinuity locating at the point $x = 0$. The spatial gradient of $\phi(x)$ is

$$\phi_{,x}(x) = \begin{cases} 1 & \text{for } x > 0 \\ -1 & \text{for } x < 0 \end{cases}, \quad (7)$$

where the comma representing the gradient operator. The use of the distance function leads to suboptimal rate of convergence for material interface problems (Sukumar et al., 2001). A subsequent advance – use of the ridge enrichment function (Moës et al., 2003) for material interfaces – yielded optimal convergence rates without the presence of blending elements. Further discussions on the convergence rate and patch test can be found in Sukumar

et al. (2015). However, the distance or ridge function is only applicable for isolated faults. The goal of this work is to propose an effective and easily implemented enrichment scheme to model branched and intersecting faults.

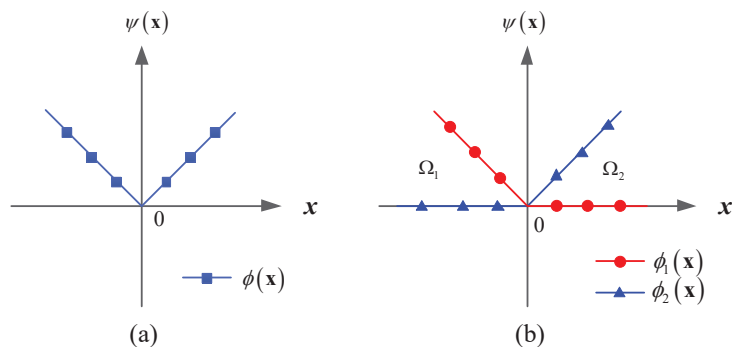


Figure 3: Enrichment functions for the case of weak discontinuities (a) distance function; and (b) the ramp functions. The discontinuity is located at $x = 0$.

Inspired by Simone et al. (2006), we establish a new enrichment scheme for case of the fault with multiple branches (the number of branches is n). First, we also divide the union of all the nodal supports completely cut by the fault into n regions $\Omega_\alpha (\alpha = 1, 2, \dots, n)$ according to the configuration of the fault, as shown in the Fig. 2(c). Then, each domain is assigned a positive distance function defined as:

$$\phi_\alpha(\mathbf{x}) = \begin{cases} \min \|\mathbf{x} - \bar{\mathbf{x}}\|_{\bar{\mathbf{x}} \in (\partial\Omega_\alpha \cap \Gamma^c)} & \text{if } \mathbf{x} \in \Omega_\alpha \\ 0 & \text{otherwise} \end{cases}, \quad (8)$$

where $\partial\Omega_\alpha$ representing the boundary of the region Ω_α . Unlike the enrichment functions for strong discontinuities, we have

$$\sum \phi_\alpha(\mathbf{x}) \neq 1 \quad \forall \mathbf{x} \in \Omega \quad (9)$$

Therefore, using a linear combination of $\phi_\alpha(\mathbf{x})$, we can construct a continuous enriched function with discontinuous derivatives reflecting the configuration of the weak fault. The expression of the enriched function is

$$\psi(\mathbf{x}) = \sum_{\alpha=1}^n c_\alpha \phi_\alpha(\mathbf{x}) \quad (10)$$

where c_α are dimensionless coefficients. In view of (1), $c_\alpha a_J \mapsto a_{\alpha J}$ works as the enriched DOF. Note that it is not required to prescribe a value of c_α since we compute and only care about the unknown $a_{\alpha J}$.

For clarity, consider the simplest one-dimensional problem. As shown in Fig. 3(b), the weak discontinuity is at $x = 0$, and hence Γ^c is the point $x = 0$. Accordingly, the whole domain Ω can be partitioned into two regions, i.e., $\Omega_1 : x < 0$ and $\Omega_2 : x > 0$, and both $\partial\Omega_1$ and $\partial\Omega_2$ contain the point $x = 0$. Therefore, the region of $\partial\Omega_\alpha \cap \Gamma^c$ is the origin and the curve of ϕ_α ($\alpha = 1, 2$) can be easily drawn as shown in Fig. 3(b). As expressed in (10), the enriched function is $c_1\phi_1(x) + c_2\phi_2(x)$. In particular if $c_1 = c_2$, the enriched function becomes $\phi(x)$ adopted in Sukumar et al. (2001) since

$$\phi_1(x) + \phi_2(x) = \phi(x) \quad \forall \mathbf{x} \in \Omega. \quad (11)$$

Fig. 4 shows the examples of enrichment functions obtained by (10) with $c_i = 1$ ($i = 1, \dots, n$), for the branched and intersecting faults crossing isoparametric quadrilateral elements. It can be seen that the functions are continuous with discontinuous derivatives within the elements, as needed.

In general, if the fault has n branches, the approximation of $\mathbf{u}(\mathbf{x})$ within

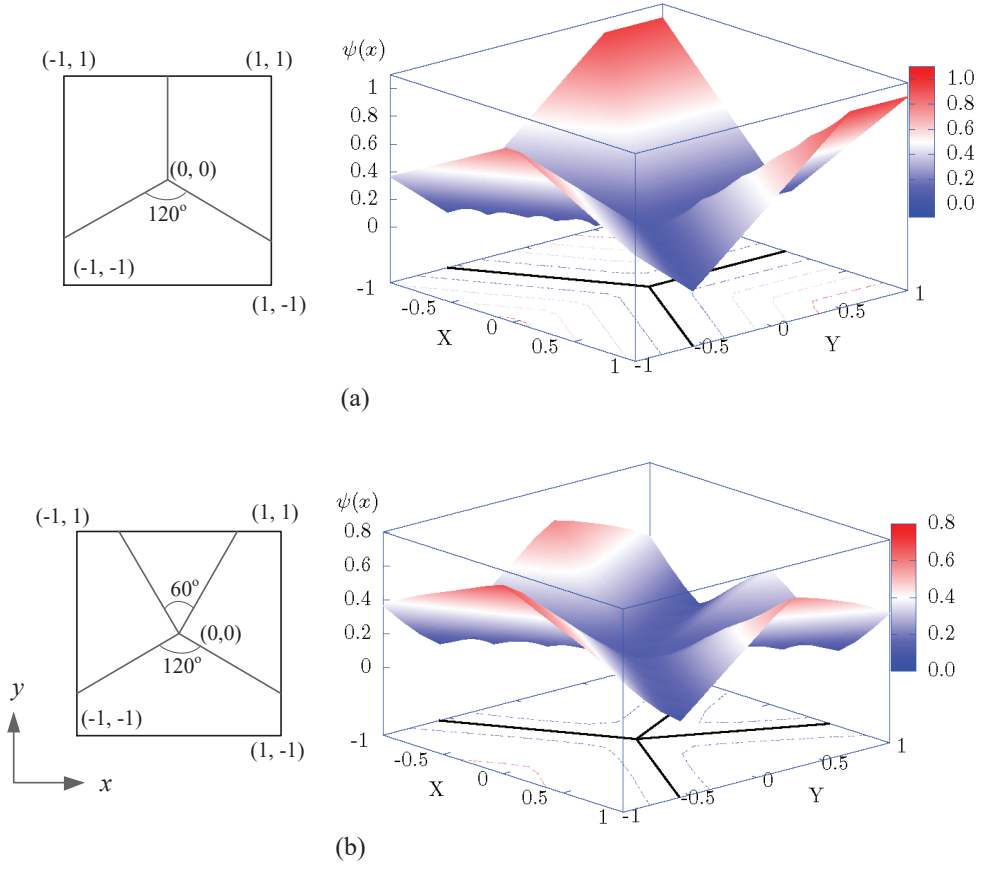


Figure 4: Examples of enriched functions within isoparametric quadrilateral elements for (a) the branched fault and (b) the intersecting fault.

the element fully cut by the fault is

$$\mathbf{u}_e^h(\mathbf{x}) = \sum_I N_I(\mathbf{x}) \left[\mathbf{u}_I + \sum_{\alpha=1}^n \phi_\alpha(\mathbf{x}) \mathbf{a}_{\alpha I} \right] \quad (12)$$

where $\phi_\alpha(\mathbf{x})$ is the distance function of the region Ω_α defined in (8) and $\mathbf{a}_{\alpha I}$ is the enriched DOF. For simplicity, the issue of blending elements is not addressed since it does not adversely affect coarse-mesh accuracy, which is the focus in this paper.

3. Branched and Intersecting Faults in Reservoir-geomechanical Models

Prévost and Sukumar (2016) studied isolated faults in a three-dimensional reservoir-geomechanical model. Here, for the sake of completeness, we briefly present the key features of the model and focus on the modeling of branched and intersecting faults. Further details can be found in Prévost and Sukumar (2016).

3.1. Field equations

For an isothermal fully saturated porous medium, the physical governing equations are the momentum conservation of the mixture and the pressure equation (Coussy, 2004), i.e.,

$$\sigma_{ij,j} + \rho g_i = 0, \quad (13)$$

$$\frac{\dot{p}^f}{M} + q_{i,i}^f + bv_{j,j}^s = 0, \quad (14)$$

where σ_{ij} is total stress tensor, ρ is the density of mixture, g_i is the gravity acceleration vector, \dot{p}^f is the time derivative of pressure, $1/M = 1/N + \phi/K_f$ with $1/N = (b - \phi)/K_s$, b is the Biot's coefficient, ϕ is the porosity, K_s and K_f are the bulk moduli of solid grain and fluid, respectively, q_i^f is the Darcy flux and defined as

$$q_i^f = -\frac{k_{ij}}{\mu^f} \left(p_{,j}^f - \rho^f g_j \right), \quad (15)$$

where k_{ij} is the component of permeability tensor, μ^f is the fluid dynamic viscosity and ρ^f is the density of fluid. The Galerkin weak forms of (13) and

(14), written for node I in element e , are given as follows:

$$\int_{\Omega_e} (\sigma_{ij,j} + \rho g_i) \tilde{N}_I d\Omega = 0, \quad (16)$$

$$\int_{\Omega_e} \left(\frac{\dot{p}^f}{M} + q_{i,i}^f + b v_{j,j}^s \right) \tilde{N}_I d\Omega = 0, \quad (17)$$

where $\tilde{N}_I(\mathbf{x}) = N_I(\mathbf{x})$ for the standard DOFs and $\tilde{N}_I(\mathbf{x}) = N_I(\mathbf{x})\psi(\mathbf{x})$ for the enriched DOFs. The unknown variables are solid displacement $\mathbf{u}(\mathbf{x})$ and pressure $p^f(\mathbf{x})$. Simultaneous integration of the stress and pressure equations is achieved by computing the coupled Jacobian matrix via finite-differencing of the residuals (Preisig and Prévost, 2012; Prévost and Sukumar, 2016). The fully implicit time integration scheme is employed. We use vertex centered schemes (bilinear interpolants) for both displacement and pressure. A stabilized scheme for pressure is also adopted to counter the violation of LBB requirements. Further details can be found in Preisig and Prévost (2011) and Prévost (2014).

3.2. X-FEM for Branched and intersecting faults

Now, we only consider the element e containing the intersection point of the branched or intersecting fault since there is nothing special for the enrichment of the element crossed by one branch. The approximation of the physical field $f(\mathbf{x})$ in the element e is

$$f(\mathbf{x}) = \sum_I N_I(\mathbf{x}) \left[f_I + \sum_{\alpha=1}^n \psi_\alpha(\mathbf{x}) \hat{f}_{\alpha I} \right], \quad (18)$$

where f_I is the standard DOF for node I , $\hat{f}_{\alpha I}$ is the enriched DOF corresponding to the enriched function $\psi_\alpha(\mathbf{x})$, and n is the number of enrichment functions.

For solid, the fault is a strong discontinuity of displacement, leading to $f(\mathbf{x}) = \mathbf{u}(\mathbf{x})$, $\psi_\alpha(\mathbf{x}) = H_\alpha(\mathbf{x})$ defined as (3), and $n = 2$ for the branched fault and $n = 3$ for the intersecting fault.

For fluid, when the fault is a barrier for fluid flow, we have $f(\mathbf{x}) = p^f(\mathbf{x})$, $\psi_\alpha(\mathbf{x}) = H_\alpha(\mathbf{x})$ defined as (3), $n = 2$ for the branched fault, and $n = 3$ for the intersecting fault. However if the fault is a flow conduit, we have $f(\mathbf{x}) = p^f(\mathbf{x})$, $\psi_\alpha(\mathbf{x}) = \phi_\alpha(\mathbf{x})$ defined as equation 8, $n = 3$ for the branched fault, and $n = 4$ for the intersecting fault.

4. Numerical Examples

In this section, five problems are considered. We first test our model for symmetric fluid flows. Second, we consider a complex fault consisting of branched and intersecting faults and compare the results obtained by the FEM and the X-FEM to show the efficiency of our method. Third, we present the different sliding phenomena for branched and intersecting faults. We then study a fully-coupled problem. Lastly, we check our model for three-dimensional fluid flows.

4.1. Symmetric fluid flows

We first check the enrichment schemes for symmetric problems. As shown in Fig. 5, three different symmetric faults, i.e., branched, coplanar intersect-

ing and non-coplanar intersecting faults, are embedded in the regions with $10 \times 10 \text{ m}^2$. The length of each branch (from the intersecting point to the end of each branch) is identical as 2.5 m. No flow is assumed to take place on both lateral boundaries and a free-flow boundary is used at the bottom. An inflow fluid flux $q^f = 10^{-3} \text{ m}^3/\text{s}$ is prescribed on the top boundary. The mobility of rock is $k_{\text{rock}} = 3.33 \times 10^{-8} \text{ m}^3 \cdot \text{s}/\text{kg}$, the fluid density is $1000 \text{ kg}/\text{m}^3$, and the porosity is 0.3. When the fault works a barrier for fluid flow, the longitudinal and transverse mobilities for the fault are $k_n = k_t = 10^{-2} k_{\text{rock}}$, while for fluid flow conduits $k_n = 10^{-2} k_{\text{rock}}$ and $k_t = 10^2 k_{\text{rock}}$. The code requires to prescribe the type of faults as an input and it cannot automatically determine the enriching functions according to the input hydraulic mobilities. We employ structured quadrilateral elements and the number of elements is $15 \times 15 = 265$.

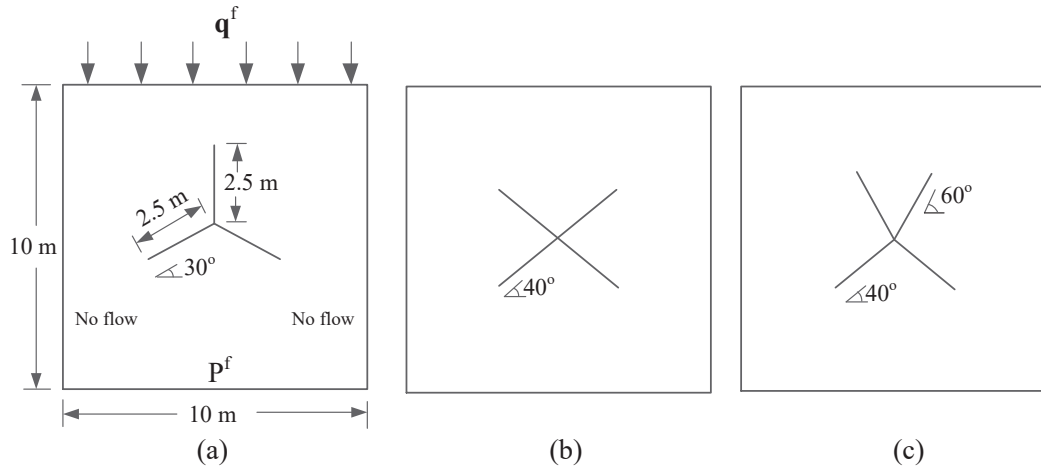


Figure 5: Geometries and boundary conditions for symmetric problems.

Fig. 6 shows the distributions of pressure and Darcy's velocity for the

sealing faults (strong discontinuities). We can see that the pressures are symmetrically distributed. Across the faults, the pressures are discontinuous. Since the faults work as barriers for fluid flow, the fluid velocities in the regions far from the faults are much larger than the regions near the faults.

For the faults as a flow conduit, we propose a new enrichment scheme for branched and intersecting weak discontinuities. When the faults work as internal fluid flow conduits that allow fluid flow in the faults as well as to enter/leave the fault, the pressure should be continuous across the fault. Fig. 7 shows the distributions of pressure and Darcy's velocity for these weak discontinuities. We can see that the distributions of pressure are symmetric and continuous. Since the longitudinal permeability of the fault is much larger than the permeability of the rock, the pressure is nonuniform. The fluid tends to flow along the fault and the fluid velocity along the fault is much larger than other regions and directions. In summary, we can obtain symmetric results for symmetric problems of strong and weak discontinuities.

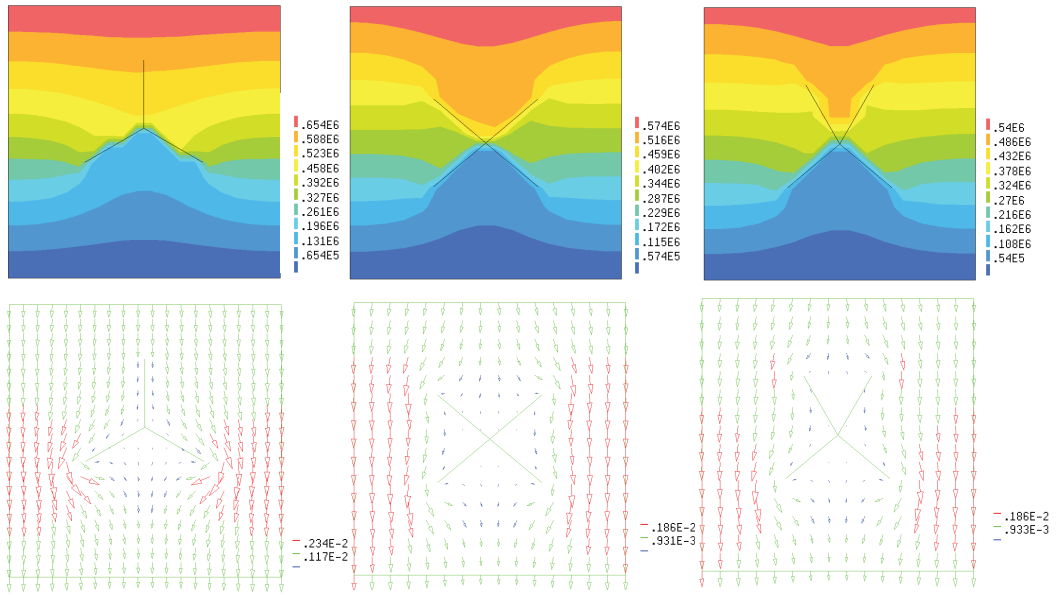


Figure 6: Distributions of pressure (Pa) and Darcy's velocity (m/s) for strong discontinuities.

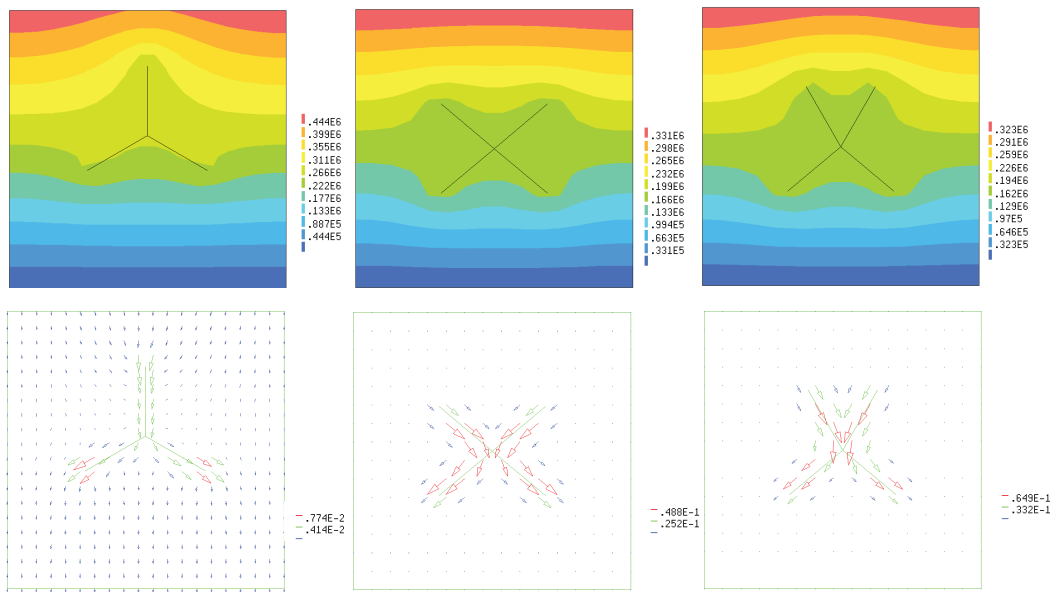


Figure 7: Distributions of pressure (Pa) and Darcy's velocity (m/s) for weak discontinuities.

4.2. Fluid flow in a region with a complex fault

In reality, the faults arbitrarily touch and intersect with each other, leading to very complex configurations. Fig. 8 shows a representative configuration of faults consisting of branched and intersecting faults. The main fault slopes at 60° , one secondary fault perpendicularly intersects the main fault, and the other secondary fault perpendicularly touch the main fault. We reemphasize that there is no need to preprocess the hierarchy of these faults since the branches are independent and only used to divide the region into several domains. The boundary conditions and the material parameters are identical to those in the last example.

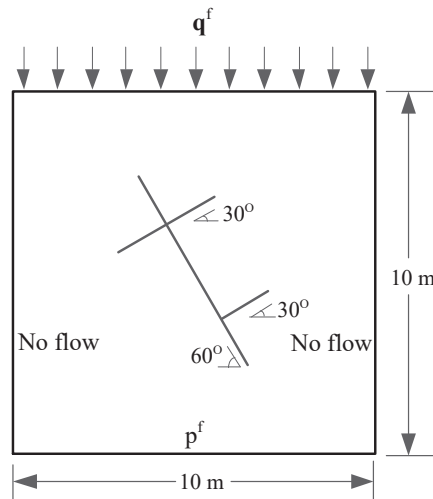


Figure 8: Geometry and boundary conditions for fluid flow within a region with a complex fault.

To evaluate the performance of the X-FEM in terms of efficiency and accuracy, we conducted the numerical simulations using the FEM with a

conformal mesh and compared the results. As shown in Fig. 9a, the conformal mesh used in the FEM consists of 13,435 nodes and 26,788 triangular elements (25,076 for the domain and 1,712 for the fault). The fault thickness is set as 5 cm and the fault permeability in the global axes is computed by performing the rotation of the fault local permeability with transverse and longitudinal permeability respectively, to the reference axes of the domain. The same problem is solved with the X-FEM pressure option using a structured quadrilateral mesh. As illustrated in Fig. 9b, only $15 \times 15 = 225$ elements are adopted. We find that all the enrichment schemes are required for the enrichment of the nodes, e.g., enriched by one branch, multiple branches, branched fault, and intersecting fault.

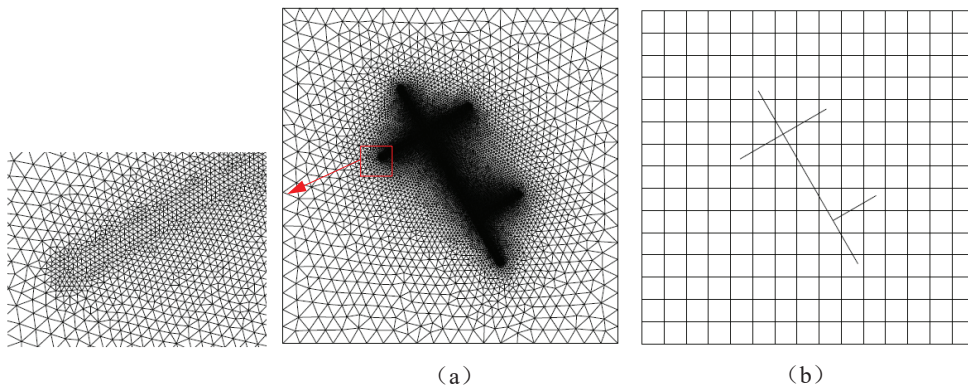


Figure 9: Meshes used in the FEM (a) and the X-FEM (b).

Fig. 10 shows the distributions of pressure for different cases: (a) sealing faults with the FEM, (b) strong discontinuities with the X-FEM, (c) faults working as flow conduits with the FEM, and (d) weak discontinuities with

the X-FEM.

We first compare the results for strong discontinuities, as illustrated in Fig. 10a and Fig. 10b. There are pressure jumps across the faults for both the FEM and the X-FEM. The maximum pressure solved by the FEM is 0.60 MPa and 0.59 MPa for the X-FEM. We can see that even with such a coarse mesh the solution can be captured with sound accuracy.

For weak discontinuities, as shown in Fig. 10c and Fig. 10d, the distributions of the pressure are practically identical. However, the flow in the cross section of the fault in the FEM solution is found to be highly non-uniform, which the X-FEM procedure cannot reproduce since it lumps it into a single flow in and out of the fault channel. So the solution using X-FEM is not able to capture the details of the flow in the fault, and can only provide an average solution. That is why the maximum pressures are 0.46 MPa for the FEM versus 0.32 MPa for the X-FEM. Further discussions can be found in Prévost and Sukumar (2016). This example demonstrates the significant simplifications with reasonable accuracy of the enriched FE fault model for the fluid flow.

From this example of fluid flow within a region embedded by a complex fault, we can see that the X-FEM can easily accommodate other values as dictated by Geologist experts and renders it possible to simulate tens to hundreds of faults with complex surface topology in a real geological domain.

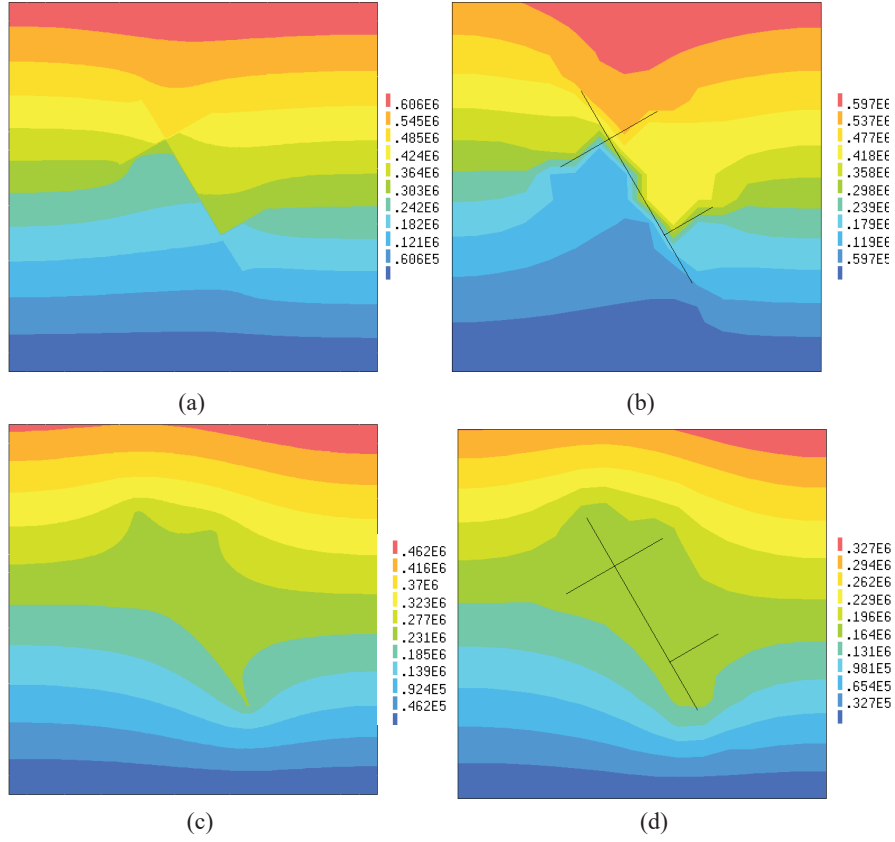


Figure 10: Distributions of pressure: (a) FEM for sealing faults; (b) X-FEM for strong discontinuity; (c) FEM for faults working as flow conduit; and (d) X-FEM for weak discontinuity.

4.3. Fault slipping

For solid, the fault always plays the role of a discontinuity of displacement, i.e., strong discontinuity of \mathbf{u} . The slipping of the fault is considered by the Mohr-Coulomb criterion. As shown in Fig. 11, we compare the sliding of branched and intersecting faults. The domain is $10 \times 10 \text{ m}^2$. The branched fault consists of fault I with slope angle $\alpha = 60^\circ$ and length 6.66 m and horizontal fault II with length 3.33 m. We fix the right end of fault II

and elongate the fault II into 4m to get the intersecting fault, as shown in Fig. 11b. A uniform total vertical surface compressive stress is applied on the top surface, i.e. $\sigma_v = 10$ MPa. The vertical displacement of bottom surface is constrained. The horizontal compressive stress applied on the lateral boundaries is $\sigma_H = \sigma_v \cdot \nu / (1 - \nu)$, where $\nu = 0.25$ is the Poisson's ratio. So the horizontal compressive stress is $\sigma_H \approx 3.33$ MPa. The Young's modulus is $E = 30$ GPa. A structured mesh is adopted, and the total number of elements is $19 \times 19 = 361$. For the cohesionless material, the critical friction angle for isolated fault is $\phi = \alpha / 2 = 30^\circ$. Here we set the friction angle as 24° .

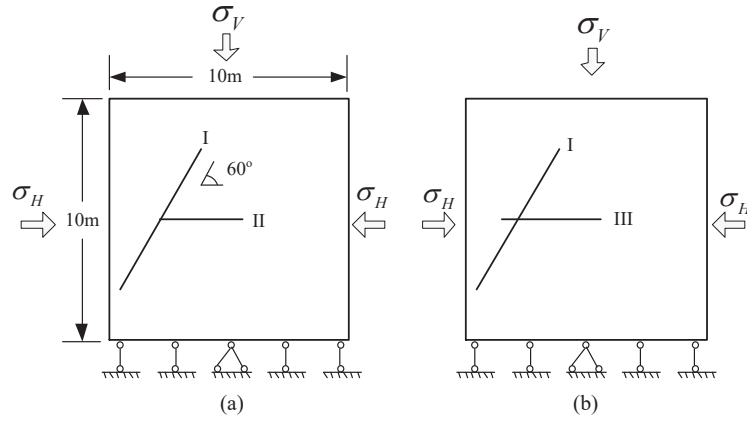


Figure 11: Geometry and boundary conditions for failure analysis: (a) branched fault and (b) intersecting fault. The lengths for faults I, II and III are 6.66m, 3.33m, and 4m, respectively.

The resulting displacement vectors for the branched and intersecting faults are shown in Fig. 14a and Fig. 14b, respectively. We can see that an obvious slide along the sloping fault occurs for the branched fault, and the

horizontal branch does not affect the sliding. However, for the intersecting fault, the displacement field is different with that for the branched fault. It seems that the horizontal fault hinders the slipping of the slopping branch and the maximum magnitude of displacement for the intersecting fault is smaller than the branched fault. We may conclude that the intersecting fault is more stable than the branched fault. Through this example, we can see that the X-FEM can accurately simulate the slipping of branched and intersecting faults.

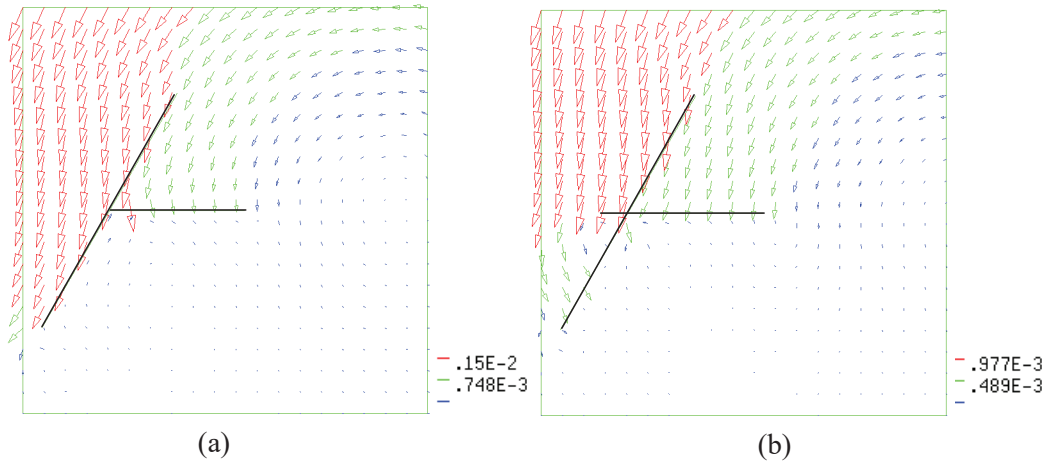


Figure 12: Displacement vectors for (a) branched fault and (b) intersecting fault.

4.4. Fully-coupled reservoir-geomechanics model

In this case, we consider a fully-coupled reservoir-geomechanics model to show the fault slipping triggered by an injection excess pressure. As shown Fig. 13, the geometry of the branched fault is identical to the last case (Fig. 11a). The effective compression applied on the top surface is $\sigma'_v = 20$ MPa and the effective confining pressure for the left and right boundaries

are $\sigma'_H = K\sigma'_v = 6.67 \text{ MPa}$ with $K = \nu / (1 + \nu)$. Here the Poisson's ratio is still $\nu = 0.25$, which means the critical friction angle would be $\phi_{\text{crit}} = 30^\circ$. The hydraulic pressure on the top surface is set as $p_0^f = 10 \text{ MPa}$, the other boundaries are impermeable. The pressure at the injection point is set as $p^f = 15 \text{ MPa}$ with 5 MPa excess pressure.

Since the novelty of this work is to handle weak discontinuities with complex configurations, the fault is viewed as a fluid conduit by setting the mobilities of the fault as $k_t = 10^2 k_{\text{rock}}$ and $k_n = k_{\text{rock}}$, where $k_{\text{rock}} = 3.6 \times 10^{-3} \text{ m}^3 \cdot \text{h} / \text{kg}$. Note that the fault is always a strong discontinuity for the displacement. The friction angle is set as $\phi = 40^\circ > \phi_{\text{crit}}$ to ensure that the fault slipping is triggered by the injection pressure.

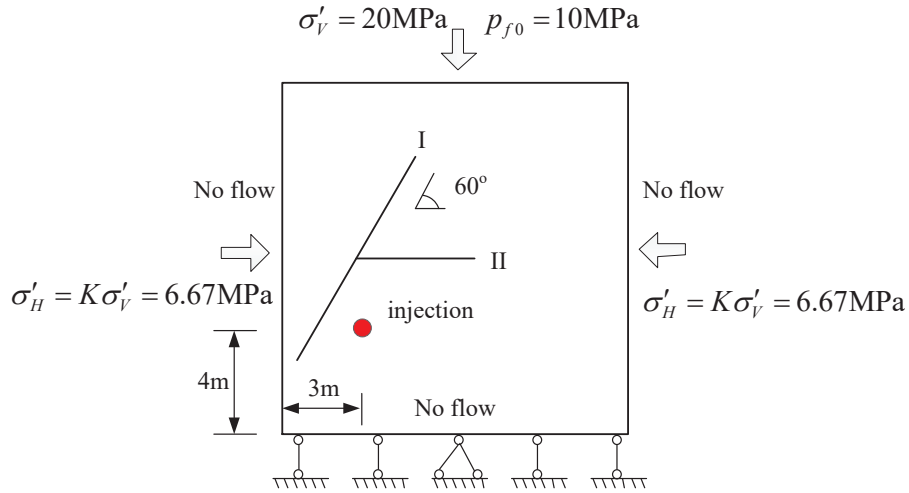


Figure 13: Geometry and boundary conditions for a fully-coupled reservoir-geomechanics model.

Fig. 14 shows the results after injecting for 10 hours. Since the fault is

modeled as a weak discontinuity for the pressure, the distribution of pressure is continuous. As shown in Fig. 14b, the fault slips due to the increase of hydraulic pressure. The versatility of the proposed enrichment scheme is demonstrated by the fully-coupled model.

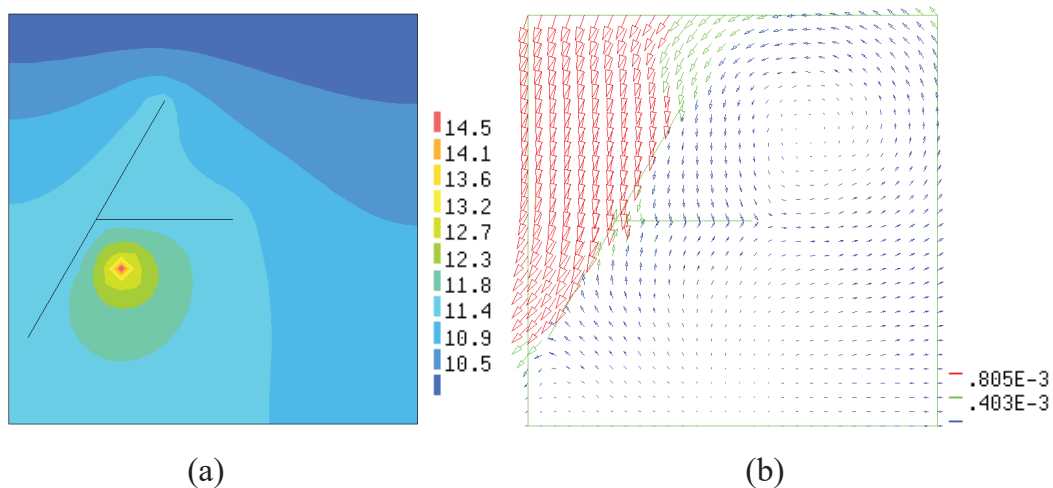


Figure 14: Results after injecting excess pressure for 10 hours with (a) distribution of pressure (MPa) and (b) displacement vectors.

4.5. Fluid flow in 3D

As the final example, we evaluate the effectiveness of the proposed enrichment scheme for weak discontinuities in 3D problems. The results for strong discontinuities are also shown. As shown in Fig. 16, we extrude the sample shown in Fig. 5a along the vertical direction of the plane to generate a 3D branched model. No flow is assumed to take place on both lateral boundaries and a free-flow boundary is used at the bottom. An inflow fluid flux $q^f = 10^{-3} \text{ m}^3/\text{s}$ is prescribed on the top boundary. The mobility of the rock is $k_{\text{rock}} = 3 \times 10^{-9} \text{ m}^3 \cdot \text{s}/\text{kg}$, the fluid density is $1000 \text{ kg}/\text{m}^3$, and the porosity

is 0.3. When the fault works as a barrier for fluid flow, the longitudinal and transverse mobilities for the fault are $k_n = k_t = 10^{-2}k_{\text{rock}}$, while for fluid flow conduits $k_n = k_{\text{rock}}$ and $k_t = 10^3k_{\text{rock}}$. We employ structured hexahedral elements and the number of elements is $19 \times 19 \times 19 = 6859$.

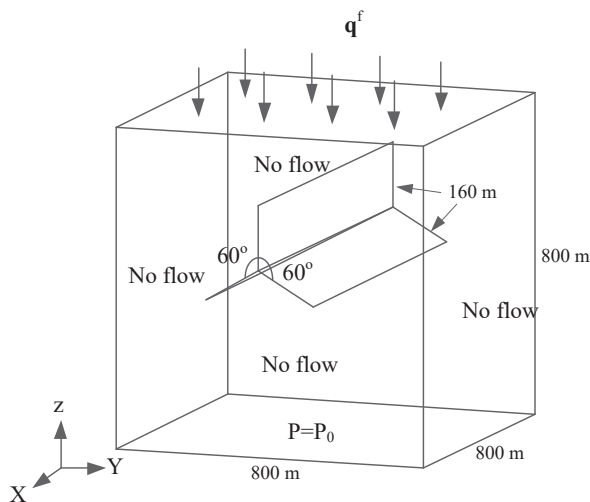


Figure 15: Geometry and boundary conditions for 3D fluid flows.

Fig. 16 shows the distributions of pressure and Darcy's velocity for the strong and weak discontinuities. We can see that the pressures are symmetrically distributed for both cases. When the fault is a strong discontinuity for fluid flow, there are pressure jumps across the faults and the fluid flows circumventing the faults. However, when the fault is a weak discontinuity, the pressure is continuous and the fluid tends to flow along the fault and the fluid velocity along the fault is much larger than other regions and directions. Since the enrichment schemes for the branched and intersecting faults are the same, the example with a branched fault is sufficient to show the

effectiveness of the new enrichment scheme for weak discontinuities in 3D.

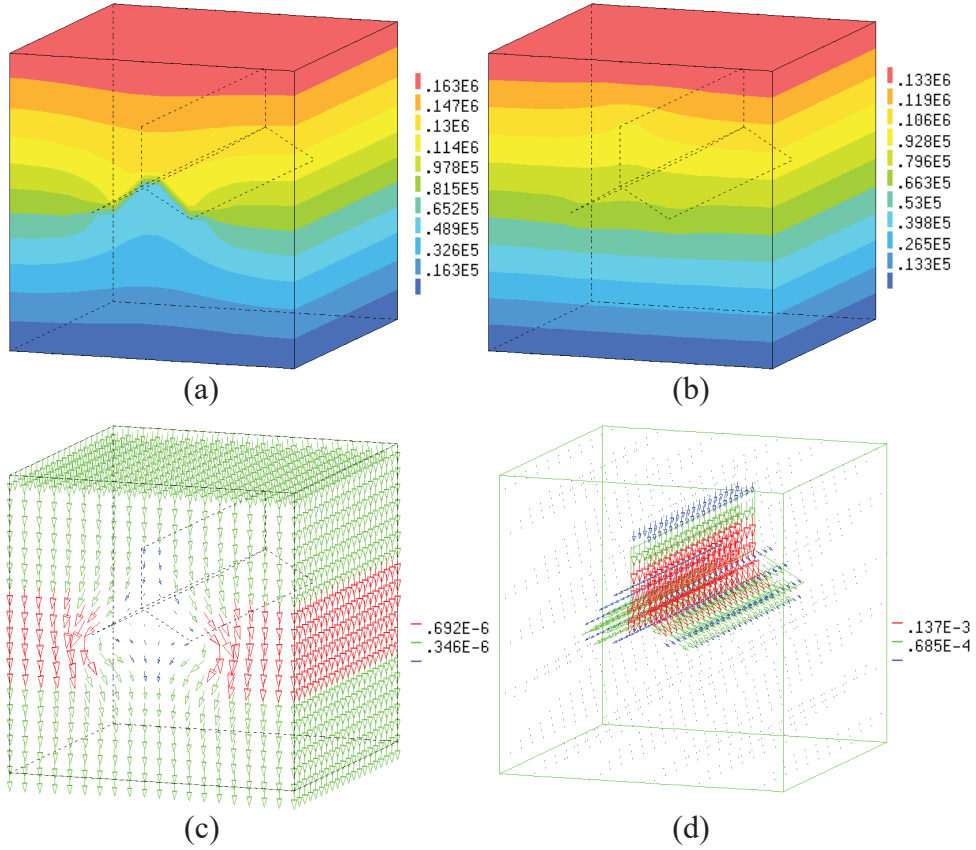


Figure 16: Results for 3D fluid flows: (a) pressure distribution for strong discontinuities, (b) pressure distribution for weak discontinuities, (c) fluid velocity vectors for strong discontinuities, and (d) fluid velocity vectors for weak discontinuities.

5. Conclusion

In this work, we described the modeling of branched and intersecting faults (strong and weak discontinuities) using the extended finite element method. Since the faults can play roles of fluid flow conduits (weak discontinuity), which allow fluid flow in the faults as well as to enter/leave the faults,

we developed a new enrichment strategy for branched and intersecting weak faults. Following the work of Simone et al. (2006), the element fully cut by a branched or intersecting fault is partitioned into several regions and each region is connected with an enrichment function whose value is the distance to the fault for a point that is within the region and 0 elsewhere. Thus the continuous enrichment functions with discontinuous gradients are linear combinations of these basis functions. The symmetric problems are first employed to check the proposed method. Fluid flows within a region embedded by a complex fault consisting of branched and intersecting faults are studied and results for strong and weak discontinuities using the X-FEM are compared to the FEM. From the simulations of slipping of various faults, the intersecting fault seems more stable than the branched fault. The fault slipping triggered by an injection pressure and fluid flows in three-dimensional are employed to show the effectiveness of the proposed enrichment strategies for branched and intersecting weak discontinuities.

In a real geological domain, hundreds of faults touch and intersect with each other leading to very complicated configurations of faults. Our goal is to conduct fault simulations that provide engineering accuracy on coarse meshes without the need to mesh the faults. The enriched FEM is a versatile tool for our needs. All 2D simulations in this work can be finished within one second and the 3D example takes 10 mins. The most time-consuming part is the computation of residual involving volume integral of discontinuous functions over elements. The integration of discontinuous functions

within the elements crossed by the branched or intersecting faults is still a challenge. A straightforward and widely used approach is to partition the subdomains separated by the crack surface into tetrahedra by introducing a centroid to perform standard integration. When the integrands are homogeneous monomials (satisfied for fluid and linearly elastic solid), the integration over each polyhedron is converted into the integration of the same monomials over the one-dimensional edges of the polyhedron by using Stokes's theorem and Euler's homogeneous function theorem. We have implemented this new integration scheme to simulate zig-zag faults (Liu et al., 2019). The new cubature scheme that does not require element-partitioning renders it possible to numerically assess the reactivation of tens to hundreds of faults with complex surface topology in a real geological domain.

6. Acknowledgements

The first author would like to thank Professor Armando Duarte in the Department of Civil and Environmental Engineering at University of Illinois at Urbana-Champaign and Professor Angelo Simone in Civil Engineering and Geosciences at TU Delft, for helpful discussions of their algorithm. Funding for this research was partially provided by Princeton University DYNAMFLOW research fund.

Reference

- T. Belytschko, N. Moës, S. Usui, and C. Parimi. Arbitrary discontinuities in finite elements. *International Journal for Numerical Methods in Engineering*, 50(4):993–1013, 2001.
- T. Belytschko, R. Gracie, and G. Ventura. A review of extended/generalized finite element methods for material modeling. *Modelling and Simulation in Materials Science and Engineering*, 17(4):043001, 2009.
- O. Coussy. *Poromechanics*. John Wiley, Chichester, England, 2004.
- C. Daux, N. Moës, J. Dolbow, N. Sukumar, and T. Belytschko. Arbitrary branched and intersecting cracks with the extended finite element method. *International Journal for Numerical Methods in Engineering*, 48:1741–1760, 2000.
- A. Hansbo and P. Hansbo. An unfitted finite element method, based on Nitsche’s method, for elliptic interface problems. *Computer Methods in Applied Mechanics and Engineering*, 191(47-48):5537–5552, 2002.
- A. Hansbo and P. Hansbo. A finite element method for the simulation of strong and weak discontinuities in solid mechanics. *Computer Methods in Applied Mechanics and Engineering*, 193(33-35):3523–3540, 2004.
- C. Q. Liu, J. H. Prévost, and N. Sukumar. Modeling piecewise planar fault discontinuities without element-partitioning in 3d reservoir-geomechanical

- models. *International Journal for Numerical and Analytical Methods in Geomechanics*, 43(2):530–543, 2019.
- V. Martin, J. Jaffré, and J. E. Roberts. Modeling fractures and barriers as interfaces for flow in porous media. *SIAM Journal on Scientific Computing*, 26(5):1667–1691, 2005.
- J. M. Melenk and I. Babuška. The partition of unity finite element method: basic theory and applications. *Computer Methods in Applied Mechanics and Engineering*, 139(1-4):289–314, 1996.
- N. Moës, M. Cloirec, P. Cartraud, and J. F. Remacle. A computational approach to handle complex microstructure geometries. *Computer Methods in Applied Mechanics and Engineering*, 192(28-30):3163–3177, 2003.
- S. E. Mousavi, E. Grinspun, and N. Sukumar. Harmonic enrichment functions: A unified treatment of multiple, intersecting and branched cracks in the extended finite element method. *International Journal for Numerical Methods in Engineering*, 85(10):1306–1322, 2011a.
- S. E. Mousavi, E. Grinspun, and N. Sukumar. Higher-order extended finite elements with harmonic enrichment functions for complex crack problems. *International Journal for Numerical Methods in Engineering*, 86(4-5):560–574, 2011b.
- M. Preisig and J. H. Prévost. Stabilization procedures in coupled porome-

- chanics problems: A critical assessment. *International Journal for Numerical and Analytical Methods in Geomechanics*, 35(11):1207–1225, 2011.
- M. Preisig and J. H. Prévost. Fully coupled simulation of fluid injection into geomaterials with focus on nonlinear near-well behavior. *International Journal for Numerical and Analytical Methods in Geomechanics*, 36(8):1023–1040, 2012.
- J. H. Prévost. Two-way coupling in reservoir–geomechanical models: vertex-centered galerkin geomechanical model cell-centered and vertex-centered finite volume reservoir models. *International Journal for Numerical Methods in Engineering*, 98(8):612–624, 2014.
- J. H. Prévost and N. Sukumar. Faults simulations for three-dimensional reservoir-geomechanical models with the extended finite element method. *Journal of the Mechanics and Physics of Solids*, 86:1–18, 2016.
- J. H. Prévost, A. M. Rubin, and N. Sukumar. Intersecting faults simulation for three-dimensional reservoir-geomechanical models. In *Poromechanics VI: Proceedings of the Sixth Biot Conference on Poromechanics*, pages 1992–1999, 2017.
- A. Simone, C. A. Duarte, and Giessen E. V. d. A generalized finite element method for polycrystals with discontinuous grain boundaries. *International Journal for Numerical Methods in Engineering*, 67(8):1122–1145, 2006.

N. Sukumar, D. L. Chopp, N. Moës, and T. Belytschko. Modeling holes and inclusions by level sets in the extended finite-element method. *Computer Methods in Applied Mechanics and Engineering*, 190(46-47):6183–6200, 2001.

N. Sukumar, J. E. Dolbow, and N. Moës. Extended finite element method in computational fracture mechanics: a retrospective examination. *International Journal of Fracture*, 196(1-2):189–206, 2015.